Dynamics of Ultrasonic and Electrostatic Friction Modulation for Rendering Texture on Haptic Surfaces

David J. Meyer* Michaël Wiertlewski † Michael A. Peshkin‡ J. Edward Colgate§

Department of Mechanical Engineering
Northwestern University
2145 Sheridan Rd, Evanston, IL 60208, USA

ABSTRACT

Surface haptic devices modulate the friction between the surface and the fingertip, and can thus be used to create a tactile perception of surface features or textures. We present modeling and experimental results on both ultrasonic and electrostatic surface haptic devices, characterizing their dynamics and their bandwidth for rendering haptic effects.

Keywords: Tactile devices and display; Wide-bandwidth force rendering; Surface haptics

Index Terms: H.5.2 [Information Systems]: User Interfaces—Haptic I/O

1 INTRODUCTION

Whether searching blindly through a pocket or scanning across a keyboard, surface texture provides essential information that allows a person to quickly assess the environment. It stands to reason that if technology could synthesize texture as it does visual displays and audio, this vital information pathway would be realized in the digital world. Texture encompasses multiple physical attributes of an object, such as its compliance, the microgeometry of its surface, and its friction properties [3, 22]. Surface roughness, an important dimension in the tactile definition of texture, is mediated by high frequency vibration produced by the interaction of the skin with the surface [2]. Measurements made on natural and sinusoidal textures show that these vibrations are high-bandwidth in nature [20, 19], with frequency content up to 800 Hz. A texture signal is comprised of many frequencies across this bandwidth, summed to form a rich waveform. This paper evaluates the technological capabilities of current surface haptic devices in rendering forces and vibrations across the working bandwidth of texture perception.

1.1 High-bandwidth haptics

Haptic rendering has often used robotic force feedback devices to modulate a force output as a function of a user's motion [14]. In order to reproduce the fine details of texture however, the rate of change of the force provided to the user must approach the capability of the somatosensory system to perceive the high frequency component of a texture signal. Campion and Hayward showed that the width of the frequency response of the device is critical for high fidelity rendering [5], and that devices should be able to render up to 500 Hz controllably. Robotic devices seldom permit this high bandwidth.

*meyerdj@u.northwestern.edu
†wiertlewski@northwestern.edu
‡peshkin@northwestern.edu
§colgate@northwestern.edu

Another approach to rendering texture focuses only on the high frequency vibration using vibrotactile devices [11, 20, 6]. These approaches generally produce high-frequency vibrations with either linear resonant actuators or wide-bandwidth actuators. Some approaches combine both rendering techniques by mounting vibrotactile actuators on a traditional force feedback display [9]. These methods attempt to recreate the wide bandwidth by rendering low frequency forces with the robotic device, and high frequency forces with the vibrotactile actuators.

Due to the popularity of touchscreen devices, surface haptic technology has gained attention in recent years. Surface haptic devices promise to render forces directly on the fingertip, a capability that could support display of realistic virtual textures.

1.2 Surface Haptics and Texture

Surface haptic devices focus on modulating or rendering forces at the interface between a fingertip and a surface. Three main physical methods of force production have emerged in surface haptic technology: moving overlays, ultrasonically vibrating surfaces, and electrostatic surfaces. Moving overlays typically use a thin film overlay on a static visual display[16, 15]. When a user touches the display, the finger is actually contacting the overlay, which is actuated using motors to produce a shear force on the fingertip.

Ultrasonic surface haptic devices create tactile percepts on a bare finger by vibrating the surface ultrasonically, reducing the fingertip contact time with the surface and thus reducing friction[17, 21, 4, 12]. While the user cannot perceive the ultrasonic vibration of the surface itself, friction between the surface and fingertip is reduced as the amplitude of the vibrations increases. Electrostatic surface haptic devices also aim to modulate surface friction, but to do so without mechanical actuation. Instead, an electric field created between the surface and the fingertip attracts the skin to the surface, increasing the normal force and thus increasing friction[1, 10, 13].

The goal of our research is to understand these surface haptic approaches with respect to their capability to render high-bandwidth forces on a fingertip. We examine both an ultrasonic display, and an electrostatic display and their respective texture rendering capabilities. We did not consider haptic overlay devices.

2 METHODS

2.1 Texture Generation via amplitude modulation

The ultrasonic friction modulation device was made from a glass rectangle of dimension 76x22x3.1 mm. It was actuated via two circular piezoelectric actuators glued on the surface of the glass. The electrostatics device was made from a glass rectangle of dimension 103x30x0.5 mm. A 40 nm layer of ITO on top of the glass served as the electrostatic actuation conductor. A 460 nm layer of insulator atop the conductor acts to prevent conduction between the finger and conductor.

Both the electrostatic and ultrasonic devices use a high-frequency signal to affect friction. The modulation of the amplitude of the carrier signal at perceptible frequencies creates texture.

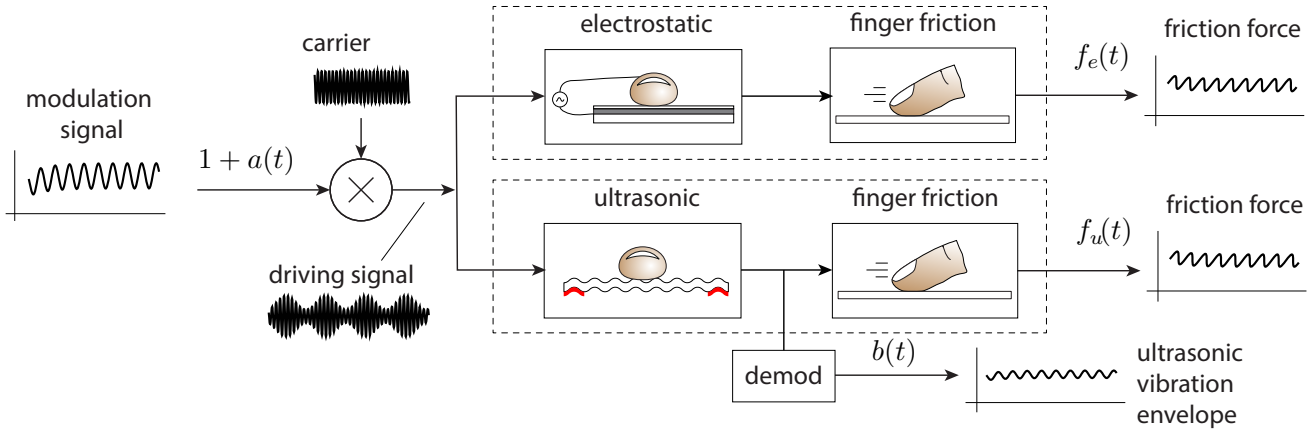

Figure 1: Block diagram of texture generation. An amplitude modulated signal is created with carrier frequency f_0 and modulation signal $a(t)$ before being used by the friction modulation device. The dynamics are studied by comparing the modulation signal to the friction force produced.

A schematic of both our displays is shown in figure 1. The carrier ($f_0 = \omega_0/2\pi$ >10 kHz) is multiplied by a modulation signal ($f_m = \omega_m/2\pi$ <1 kHz) which is used to drive the friction modulation device. In the simple case of a single modulation frequency, this results in a driving signal containing frequency components $f_0 \pm f_m$.

Electrostatic dynamics relate the driving signal to the electric field acting on the finger. Since the electrical dynamics of the display are significantly faster than the driving signal, we can assume that the driving signal directly determines the electric field. The finger friction mechanics then relate the electric field to the friction force. Due to its resonant nature, the ultrasonic display shows a more complex behavior when driven with a modulated signal. The ultrasonic screen is designed to resonate at the carrier frequency, so the dynamics in the surrounding frequency region play an important role in how the screen vibrates. Since the finger friction mechanics correlate the amplitude of vibration with friction, the ultrasonic vibration envelope is a crucial middle step in understanding the friction modulation system.

2.2 Modeling ultrasonic vibration amplitude

Following the work of Giraud et al.[7, 8], we assume that the modulation signal is a sine wave ($a(t) = \sin(\omega_m t)$), and that the surface acts like a second order system near resonance. The ultrasonic dynamics in the vicinity of the resonance are then described by the transfer function:

$$G(s) = \frac{\omega_0^2}{s^2 + \frac{\omega_0}{Q}s + \omega_0^2} \tag{1}$$

where ω_0 is the angular frequency of the carrier and Q is the Q-factor of the device. The driving signal that is input to this system is the amplitude modulated signal created with carrier ω_0 and modulation $a(t)$. In the frequency domain, this driving signal has two side bands centered about the carrier which contain the information in the modulation signal. These two off-resonance side bands are increasingly attenuated as modulation frequency increases. Assuming the modulation frequency is significantly less than the carrier frequency, this attenuation can be described by the transfer function

$$\frac{B(s)}{A(s)} = \frac{Q}{1 + \frac{2Q}{\omega_0}s} \tag{2}$$

where $B(s)$ and $A(s)$ are the Laplace transforms of $b(t)$ and $a(t)$ respectively. The transfer function mirrors that of a first order low-pass filter with a cut-off frequency of $\frac{f_0}{2Q}$. This relationship reveals a design trade-off for ultrasonic devices, as shown in figure 2. As the Q-factor of the device increases, the vibration amplitude increases, but the useful bandwidth for texture display decreases.

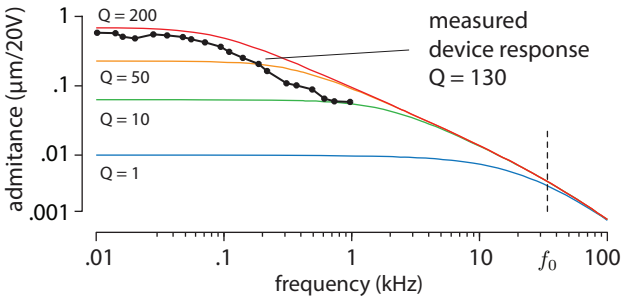

Figure 2: Bandwidth of the texture generation as a function of the Q factor of the resonant system. The black dotted curve indicates the ultrasonic device used in this experiment. Electrostatic devices are not resonant, thus do not exhibit this behavior.

2.3 Measuring ultrasonic vibration amplitude

To confirm the frequency bandwidth prediction of the model, we measured the frequency response of our ultrasonic device using a laser doppler vibrometer (PSV-400, Polytec GmbH, Waldbronn, Germany). The vibrometer measures the velocity of the ultrasonic device, perpendicular to its surface. Using a swept sine signal from 10 kHz to 50 kHz we identified the normal mode for our device to be 34.2 kHz. We determined the Q-factor by fitting a second-order equation to the frequency response. The quality factor of the ultrasonic device was found to be Q = 130.

We then drove the ultrasonic device at resonance with modulation signals varying in frequency from 10 Hz to 1000 Hz. The ultrasonic vibration envelope, $b(t)$, was calculated in post-processing using the magnitude of the Hilbert transform low-pass filtered at 2 kHz. Amplitude response between the modulation signal and the vibration envelope at each frequency is reported on the black line in figure 2 along with frequency bandwidth predictions for other Q-factors. With this method also, we found that the Q factor is close to 130. The predicted texture rendering bandwidth of the ultrasonic device used in this study is therefore around 130 Hz ($= 34.2$ kHz$/(2 \times 130)$).

2.4 Measuring fingertip friction force

We built a high-bandwidth experimental platform for measuring friction forces. Figure 3 shows a user's hand in the device. The palm of the user's hand rests on a stage that is actuated parallel and normal to the testing surface. The fingertip is pushed against the tested surface with a constant force and dragged along with a constant velocity.

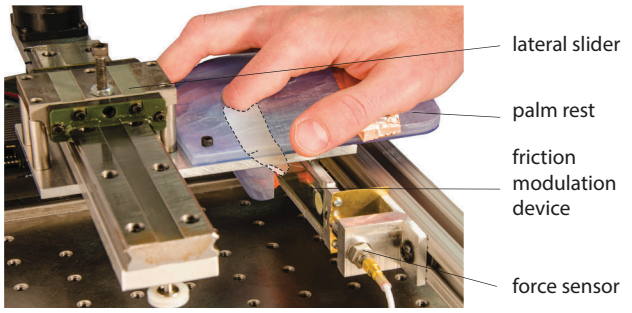

Figure 3: Image of the tribometer setup. The user's hand rests on a motorized support that drives the finger across the glass surface with a constant speed and controlled normal force. The resulting friction force is recorded with a high-bandwidth piezoelectric sensor.

The tested device is mounted on leaf springs which provide high-stiffness in the normal direction and mobility in the lateral direction. A stiff piezoelectric sensor (9203, Kistler Instrumente AG, Winterthur, Switzerland) is mounted laterally to measure the friction force. The sensing apparatus is designed to ensure a first resonance frequency higher than 1 kHz. This target frequency ensures artifact-free measurements in the frequency bandwidth relevant to tactile texture. The piezo force sensor is connected to a charge amplifier (593a, Kistler Instrumente AG, Winterthur, Switzerland).

This high-bandwidth friction force sensor platform is mounted on a slider that allows a displacement only along a direction normal to the tested device surface. A strain-gauge force sensor (Nano 17, ATI Industrial Automation, Apex, NC, USA) monitors the normal force applied to the surface. To reduce the variation in normal force, a spring is mounted in the force path. The normal force is set by pushing the finger onto the testing surface. The hand stage moves normal to the testing surface and deforms the soft spring until the nominal normal force is reached (typically 1 N). The stage has an opening that guides the index finger to a 20° angle with the surface. Another slider, actuated with a servo-controlled DC motor, drags the finger across the surface with constant but programmable speed. The displacement of the platform is measured by an optical encoder. The driving signal, friction force, and normal force are measured using a 16-bit data acquisition board at a sampling frequency of 80 kHz. The modulation signal is extracted from the measured driving signal in post-processing using the Hilbert transform for demodulation as before. The calculated modulation signal and measured forces are processed with a zero-lag low-pass filter at 2 kHz. The finger position encoder is recorded then differentiated and low-pass filtered to calculate finger velocity.

2.4.1 Protocol

Once the hand is comfortably positioned in the rest, the finger is pressed into the surface to reach the proper normal force (1 N). After a five-second settling period, the finger is dragged back and forth across the surface while friction is modulated by the device.

This basic procedure was repeated using 2 types of modulation signals, namely sinusoids and step functions. The sinusoidal friction force modulation probes the frequency response of system at frequencies from 10 to 1000 Hz. Twenty frequencies of modulation signal, equally spaced on a logarithmic scale, were tested. For every sinusoidal test, the finger was dragged with the same speed of 50 mm/s. Each frequency was repeated ten times and randomly shuffled during the experiment.

Heaviside step function waveforms were used to probe the effect of speed on the dynamics of the friction force. Each trial was repeated 20 times and averaged. Three finger speeds were tested: 22, 51 and 77 mm/s. These fall into the range of speeds normally employed in tactile exploration.

In this reported work, we focused on the mechanical behavior of friction modulation devices. We did not assess variation between skin of different individuals, or variations with temperature, moisture, or cleanliness, although these variations could be of interest. Measurements were taken with the lead author's fingertip, washed, dried, and lightly talced to maintain low moisture.

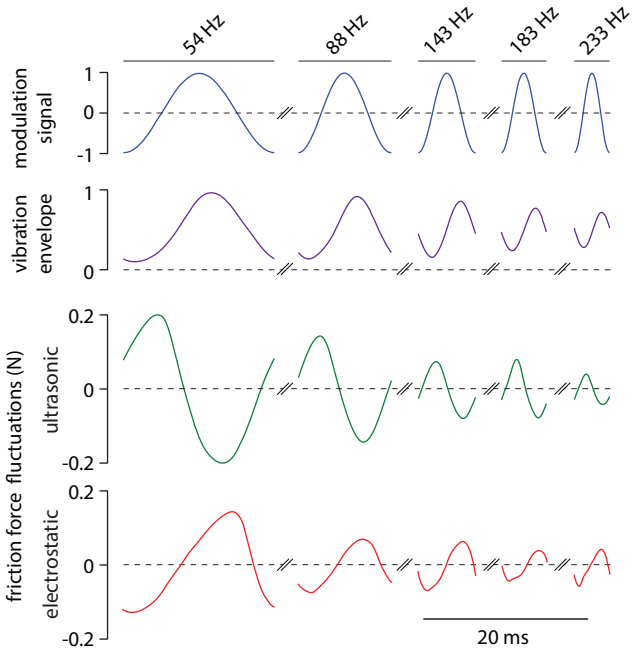

Figure 4: Response of vibration amplitude and friction force to varying frequency sine waves. As the frequency is increased beyond the cut-off frequency of 130 Hz, the vibration amplitude diminishes, and the friction modulation decays.

3 Results

3.1 Friction response to sine wave modulation

We measured the frequency response of the friction force on both ultrasonic and electrostatic displays using sinusoidal modulation signals. Each trial tested a single modulation frequency. Typical measurements for five selected frequencies are shown in figure 4. At lower frequencies the ultrasonic vibration envelope and friction force follow the modulation signal quite closely. As the frequency increases past the predicted cut-off frequency of 130 Hz, the vibration envelope begins to lag behind the modulation, and attenuate in magnitude. The friction force exhibits a small phase lag of about 20 degrees relative to the vibration envelope.

The amplitude and phase response of the friction force are extracted from these time-domain data using the ratio of the cross power spectral density to the auto power spectral density of the modulation signal. Figure 5 shows a Bode plot of these extracted responses for both ultrasonic and electrostatic displays. Each point is an average measure of 10 trials, with the standard error shown in the shaded area. For frequencies less than 100 Hz, the shape of the

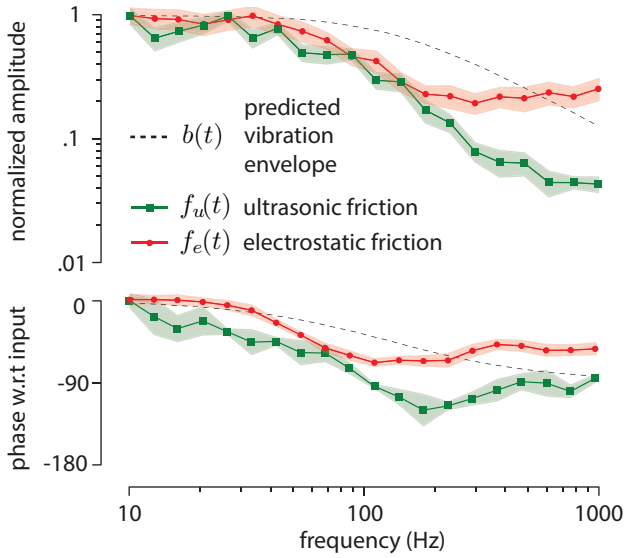

Figure 5: Frequency response of the friction modulation. Due to its resonant behavior, the ultrasonic device shows an attenuation of its amplitude with increasing frequency of the modulation signal. As a result the friction levels caused by this ultrasonic motion also decay. The electrostatic display on the other hand shows a more constant behavior across frequencies.

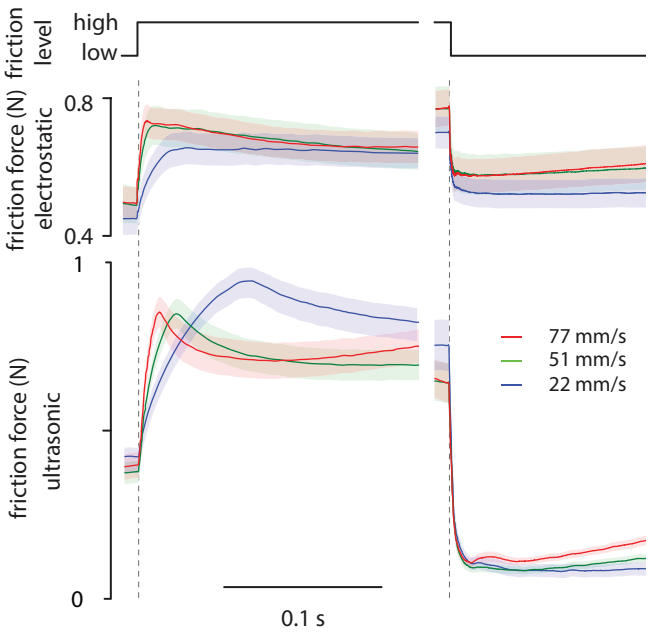

Figure 6: Response to a step change in friction level. Electrostatic devices are more responsive than ultrasonic devices. The rate of change of the force depends on the relative velocity between the finger and the device.

magnitude response is similar for both ultrasonic and electrostatic displays. At higher frequencies, the response of the ultrasonic display rolls off more rapidly, as expected. The phase information shows that the ultrasonic display exhibits a larger delay across the frequency spectrum.

3.2 Friction response to step functions

We also measured the friction force response to step functions in modulation signal on both types of display. Figure 6 shows the results for a the case of a rising and a falling step function. Traces show an average across 20 trials, while the shaded region shows the standard error. The electrostatic device shows a significantly faster response than the ultrasonic device in the rising friction case. In all cases, an overshoot dependent on velocity is observed. The transition from high to low friction corresponds to activating the ultrasonic device or turning off the electrostatic device.

4 Discussion

As a general matter, we have shown that the response of the electrostatic device is faster than that of the ultrasonic device. The predicted attenuation of the modulation signal for the ultrasonic display is observed in the frequency responses of both the friction force and the ultrasonic vibration envelope. Our results also show evidence of friction dynamics that are as yet un-modeled. These complex friction mechanics fall into three categories: fingertip specific physics, ultrasonic specific physics, and electrostatic specific physics.

Fingertip specific physics describe mechanical properties of the fingertip itself. For example, the impedance of the fingertip will play an important role in how dynamic friction force develops, regardless of the contact surface. The measured friction frequency response in this paper exhibits some degree of attenuation and delay for both electrostatic and ultrasonic displays. It is likely that this attenuation is due to fingertip impedance, as it is observed on both surfaces. In addition, the time response of the high to low friction is in the order of 5 ms which is consistent with the relaxation time of the lateral deformation the fingertip [18].

The measured step responses shown in figure 6 give insight into device-specific physics. More specifically, the rise-time of friction after an ultrasonic display is switched off shows velocity-dependent physics. The friction modulation bandwidth of the ultrasonic device was measured to be around 130 Hz, but the observed rise-time for 22 mm/s finger velocity is on the order of 70 ms, almost an order of magnitude slower than expected.

One possible cause for this slow delay is a squeeze-film, which has been proposed before as the friction-reduction mechanism on ultrasonic displays[4, 17]. It may be that at higher velocities, the squeeze-film discharge dynamics do not affect the friction transient greatly, since the finger leaves the squeeze-film behind as it traverses. At a low enough velocity though, the film of air may remain under the fingertip, discharging more slowly out the edges.

5 Conclusion

We have studied the dynamic behavior of the finger friction when using amplitude-modulated electrostatic and ultrasonic friction modulation devices. The results show that electrostatic devices are faster in the modulation of friction than the tested ultrasonic device, for both sinusoidal and step function modulation signals.

Ultrasonic devices suffer from their construction around a resonant system that limits their ability to render high-bandwidth texture. Although friction reduction on ultrasonic displays is not entirely understood, it may prove necessary to move away from resonant designs in order to achieve wide-bandwidth performance. Lowering the Q-factor, by either reducing the stored energy or increasing damping, is the key to faster ultrasonic devices. Despite slower dynamics, ultrasonic devices may provide a much wider range of friction modulation compared to electrostatic displays, going from a coefficient of friction as high as 1 to almost frictionless contact, and offer the potential to render a vast variation of stickiness sensation.

Electrostatic surface haptic displays show promise in their capability to produce wide-bandwidth forces for texture rendering. Unlike ultrasonic devices, the building up of charges that produces

the increase in friction is not limited by any resonant behavior. Sine sweep and step function both show a clear advantage of this technology to render high-frequency content and simulate rough textures. On the other hand, the range of friction level that can be produced is not as wide as for ultrasonic devices and therefore the quasi-static friction force rendering is not as rich.

Perhaps the optimal surface display for rendering texture combines both technologies. Previously demonstrated by Giraud et al[8], using the electrostatic screen as an ultrasonic device allows for both large variation of the coefficient of friction and finer and higher-frequency friction fluctuations.

ACKNOWLEDGEMENTS

This material is based upon work supported by the National Science Foundation under Grants No. IIS-0964075 and IIS-1302422. The authors would also thank Professor Royston for the use of the LDV, Jack Qiu for his help in the manufacturing of the experimental apparatus, and Mondher Cherif at Tangible Haptics LLC for providing electrostatic devices.

REFERENCES

[1] O. Bau, I. Poupyrev, A. Israr, and C. Harrison. TeslaTouch: electrovibration for touch surfaces. In *Proceedings of the 23nd annual ACM symposium on User interface software and technology*, UIST '10, page 283–292, New York, NY, USA, 2010. ACM.

[2] S. Bensmaïa and M. Hollins. The vibrations of texture. *Somatosensory & motor research*, 20(1):33–43, 2003.

[3] W. M. Bergmann-Tiest and A. M. L. Kappers. Analysis of haptic perception of materials by multidimensional scaling and physical measurements of roughness and compressibility. *Acta Psychologica*, 121(1):1–20, 2006.

[4] M. Biet, F. Giraud, and B. Lemaire-Semail. Squeeze film effect for the design of an ultrasonic tactile plate. *IEEE Transactions on Ultrasonics, Ferroelectrics and Frequency Control*, 54(12):2678–2688, 2007.

[5] G. Campion and V. Hayward. Fundamental limits in the rendering of virtual haptic textures. In *Proceedings of the First Joint Eurohaptics Conference and Symposium on Haptic Interfaces for Virtual Environment and Teleoperator Systems*, page 263–270, 2005.

[6] H. Culbertson, J. M. Romano, P. Castillo, M. Mintz, and K. J. Kuchenbecker. Refined methods for creating realistic haptic virtual textures from tool-mediated contact acceleration data. In *Haptics Symposium (HAPTICS), 2012 IEEE*, page 385–391, 2012.

[7] F. Giraud, M. Amberg, and B. Lemaire-Semail. Design and control of a haptic knob. *Sensors and Actuators A: Physical*, 2013.

[8] F. Giraud, M. Amberg, and B. Lemaire-Semail. Merging two tactile stimulation principles: Electrovibration and squeeze film effect. In *World Haptics Conference (WHC), 2013*, page 199–203, 2013.

[9] R. Howe and D. Kontarinis. High-frequency force information in teleoperated manipulation. *Experimental Robotics III*, page 341–352, 1994.

[10] J. Linjama and V. Mäkinen. E-sense screen: Novel haptic display with capacitive electrosensory interface. In *HAID 2009, 4th Workshop for Haptic and Audio Interaction Design*, Dresden, Germany, 2009.

[11] T. Maeno, K. Otokawa, and M. Konyo. Tactile display of surface texture by use of amplitude modulation of ultrasonic vibration. In *Proceedings of the IEEE Ultrasonics Symposium*, page 62–65, 2006.

[12] N. Marchuk, J. Colgate, and M. Peshkin. Friction measurements on a large area TPaD. In *Haptics Symposium, 2010 IEEE*, pages 317 –320, Mar. 2010.

[13] D. J. Meyer, M. A. Peshkin, and J. Colgate. Fingertip friction modulation due to electrostatic attraction. In *World Haptics Conference (WHC), 2013*, pages 43–48, 2013.

[14] M. Minsky and S. Lederman. Simulated haptic textures: Roughness. In *Proceedings of the ASME Dynamic Systems and Control Division*, volume 58, page 421–426, 1996.

[15] A. Roudaut, A. Rau, C. Sterz, M. Plauth, P. Lopes, and P. Baudisch. Gesture output: eyes-free output using a force feedback touch surface. In *Proceedings of the SIGCHI Conference on Human Factors in Computing Systems*, CHI '13, page 2547–2556, New York, NY, USA, 2013. ACM.

[16] D. Wang, K. Tuerz, M. Rossi, and J. Shu. Haptic overlay device for flat panel touch displays. In *12th International Symposium on Haptic Interfaces for Virtual Environment and Teleoperator Systems, 2004. HAPTICS '04. Proceedings*, pages 290–, 2004.

[17] T. Watanabe and S. Fukui. A method for controlling tactile sensation of surface roughness using ultrasonic vibration. In *Robotics and Automation, 1995. Proceedings., 1995 IEEE International Conference on*, volume 1, pages 1134 –1139 vol.1, May 1995.

[18] M. Wiertlewski and V. Hayward. Mechanical behavior of the fingertip in the range of frequencies and displacements relevant to touch. *Journal of Biomechanics*, 45(11):1869–1874, July 2012.

[19] M. Wiertlewski, C. Hudin, and V. Hayward. On the 1/f noise and non-integer harmonic decay of the interaction of a finger sliding on flat and sinusoidal surfaces. In *World Haptics Conference (WHC), IEEE*, pages 25 –30, June 2011.

[20] M. Wiertlewski, J. Lozada, and V. Hayward. The spatial spectrum of tangential skin displacement can encode tactual texture. *IEEE Transactions on Robotics*, 27(3):461–472, 2011.

[21] L. Winfield, J. Glassmire, J. E. Colgate, and M. Peshkin. T-PaD: tactile pattern display through variable friction reduction. In *EuroHaptics Conference, 2007 and Symposium on Haptic Interfaces for Virtual Environment and Teleoperator Systems. World Haptics 2007. Second Joint*, pages 421 –426, Mar. 2007.

[22] T. Yoshioka, S. Bensmaia, J. Craig, and S. Hsiao. Texture perception through direct and indirect touch: An analysis of perceptual space for tactile textures in two modes of exploration. *Somatosensory & motor research*, 24(1-2):53–70, 2007.